Letter

Unraveling the excitonic states in bulk $2H$-MoS_2 via their giant Stark shift

Vishwas Jindal,[1] Thorsten Deilmann,[2,*] and Sandip Ghosh[1,†]

[1]*Department of Condensed Matter Physics and Materials Science, Tata Institute of Fundamental Research, Homi Bhabha Road, Mumbai 400005, India*

[2]*Institut für Festkörpertheorie, Westfälische Wilhelms-Universität Münster, 48149 Münster, Germany*

(Received 17 March 2023; revised 17 May 2023; accepted 19 May 2023; published 2 June 2023)

The interlayer exciton (IL) in bilayer $2H$-MoS_2 has earlier been shown to undergo large Stark splitting under electric field $F_z \parallel \mathbf{c}$ axis. We show that the excited state exciton A_{2s} in bulk $2H$-MoS_2 undergoes nearly three times as large splitting, with a dipole moment magnitude 1.46 enm. The nature and evolution of different exciton species with F_z is verified by comparison with *ab initio* GW-Bethe-Salpheter equation (BSE) calculations that include the full electron-hole correlations. The excitonic wave functions reveal the individual character of the exciton states at high F_z as the ground state A_{1s}, split interlayer IL_-, IL_+, and split excited state A_{2s-}. Extrapolation to low F_z indicates that IL and A_{2s} mix strongly. We try to rationalize the large dipole moment values by comparing GW-BSE results with the hydrogenic exciton model. Although the dominant A_{1s} shows an insignificant Stark shift, its large anticrossing with A_{2s-} provides a pathway for its modulation and control using an electric field.

DOI: 10.1103/PhysRevB.107.L241201

Introduction. Excitons in transition-metal dichalcogenide (TMD) semiconductors of the type MX_2 (M=Mo and W, and X=S, Se, and Te), which can form stable mono/few-layer films, have large oscillator strengths and large binding energies that exceed thermal energy $k_BT \sim 26$ meV at room temperature. Consequently, excitons dominate the optical spectrum of TMDs. Many of the new electronic structure related properties discovered in TMDs in recent years, such as spin-valley coupling [1], spin-layer locking [2], nonradiative dark states [3], are manifest through excitons, which have been studied extensively [4]. Unlike typical group III–V semiconductors, the presence of excitons at room temperature in TMDs makes their study important for any optoelectronic device application [5]. In this context, there have been several studies, which investigated the response of excitons in few-layer TMDs to electric fields. In monolayer WS_2, films energy of the ground-state A_{1s} exction and its charged counterpart the trion, could be tuned indirectly by ∼20 meV through influencing their binding energy via a gate voltage-induced change in the background carrier concentration [6]. Large changes in reflectivity due to such shifts in the A_{1s} exciton in monolayer $MoSe_2$ has been demonstrated, suggesting the possibility of making electrically switchable mirrors [7]. More recently, in bi/trilayer $2H$-MoS_2 films, a newly identified exciton state called the interlayer exciton [8–10], was found to show very large Stark splitting of its transition energy under an electric-field $F_z \parallel \mathbf{c}$ axis [11–13]. This indicated a large electric dipole moment p associated with such states, that have a considerable oscillator strength. In the case of bilayer $2H$-MoS_2 Lorchat *et al.* [11] reported $p = 0.48$ enm for interlayer excitons. Leisgang *et al.* [12] found $p = 0.47$ and $p = -0.39$ enm for the two Stark split branches of the interlayer exciton and reported the anticrossing of one of the branches with the A_{1s} exciton. Peimyoo *et al.* [13] demonstrated tunability of the interlayer exciton transition energies over 70 meV with F_z ranging from −0.04 to 0.07 V/nm. Such field split interlayer exciton transitions also show up prominently in photoluminescence under the crossed circular excitation-detection mode [14]. Anomalous weaker Stark shifts of excitons have also been reported in monolayer WS_2 [15].

The above studies focused on few-layer films, however, thicker films have higher absolute reflectance (R) and are, therefore, of interest from a device application perspective especially since interlayer excitons have also been identified in bulk $2H$-MoS_2 [16]. Here, we report a study of the influence of an electric-field $F_z \parallel \mathbf{c}$ axis on excitons in bulk $2H$-MoS_2 around its direct gap at the K point of the Brillouin zone, using reflectance spectroscopy. We compare the experimental results with first-principles electronic structure calculations that take into account electron-hole Coulomb interaction in the presence of F_z. The analysis of spatial correlation of the electron-hole wave function helped us to identify the field split exciton states, one of which is found to have a surprisingly large p value. We further investigate if the hydrogenic model of an exciton can help to understand such large p values. The Letter clarifies how excited states of excitons in bulk $2H$-MoS_2 and many similar materials should be identified.

Experimental details. The $2H$-MoS_2 crystals used in this Letter are of geological origin, obtained from SPI supplies. Thin flakes were prepared for measurement by mechanical exfoliation. The carrier concentration n was determined through Hall measurements in van der Pauw geometry on flakes ∼60 nm thick with photolithographically [17] defined Al contacts. The estimated value of $n \sim 3 \times 10^{17}$ cm^{-3} at 25 K agrees well with other reports on material from this

*thorsten.deilmann@wwu.de
†sangho10@tifr.res.in

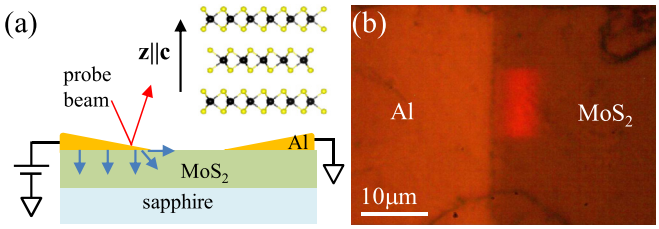

FIG. 1. (a) Arrangement for electric-field-dependent reflectance spectroscopy on bulk $2H$-MoS_2. Small arrows indicate the field direction at the Al-$2H$-MoS_2 interface. The inset is a $2H$-MoS_2 crystal structure schematic indicating the sample orientation. (b) Optical image showing the focused probe beam close to the thick edge of the Al electrode.

source [18]. For optical measurements under the electric field, Al electrodes were deposited on thick flakes by thermal evaporation in such a way that the electrodes have a gradually thinning edge see the Supplemental Material [19] as schematically shown in Fig. 1(a). R measurements were performed with the probe beam focused on the thin semitransparent part of the electrode below which the electric field is governed by the metal-semiconductor Schottky junction with field $F_z \parallel \mathbf{c}$ axis of $2H$-MoS_2. An image of the focused probe beam next to the thick edge of the electrode is shown in Fig. 1(b). For a bias of 9 V, the maximum F_z at the metal-semiconductor interface is estimated to be $\sim$0.086 V nm^{-1} see the Supplemental Material [19]. The probe beam was obtained by dispersing light from a laser driven broadband Xe light source using a 0.5-m focal length monochromator. It was focused on to the sample using a microscope arrangement with a 50× long working distance objective, resulting in a spot size of 6×12 μm^2. A lock-in amplifier was used for phase-sensitive detection of the signal from a photomultiplier tube detector. The samples were cooled using a pulse-tube He refrigerator with a sample mount designed to minimize vibrations.

Results and Discussion. Figure 2 shows the R spectrum of bulk $2H$-MoS_2 at 25 K for different bias voltages. For the lowest bias, a dominant resonant feature around 1.91 eV arising from the ground-state A_{1s} transition at the K point of the Brillouin zone of $2H$-MoS_2 is found. The smaller feature around 1.95 eV labeled $X1$ was previously identified as an interlayer (IL) exciton transition in bulk $2H$-MoS_2 [16]. There is also a weak bump around 2.0 eV labeled as $X2$. At 2.12 eV, we observe a feature due to the ground-state B_{1s} transition at the K point. With increasing voltage, $X1$ seems to redshift and gain strength, whereas $X2$ gains strength too and splits up into two features labeled IL_- and IL_+. These labelings at high fields are based on comparison with theory results to be discussed later. A_{1s} and B_{1s} energy positions seem not affected by the voltage. However, between 4 and 5 V, the $X1$ and A_{1s} show anticrossing behavior wherein $X1$ comes closest to A_{1s} gains strength and then we see it at energies below A_{1s} with diminished strength, labeled as A_{2s-}. The energy positions of these transitions marked by arrows were inferred from reflectance line-shape simulations [19]. For the $X1$ feature, we observe a Stark shift as large as 60 meV with a moderate voltage of 9 V.

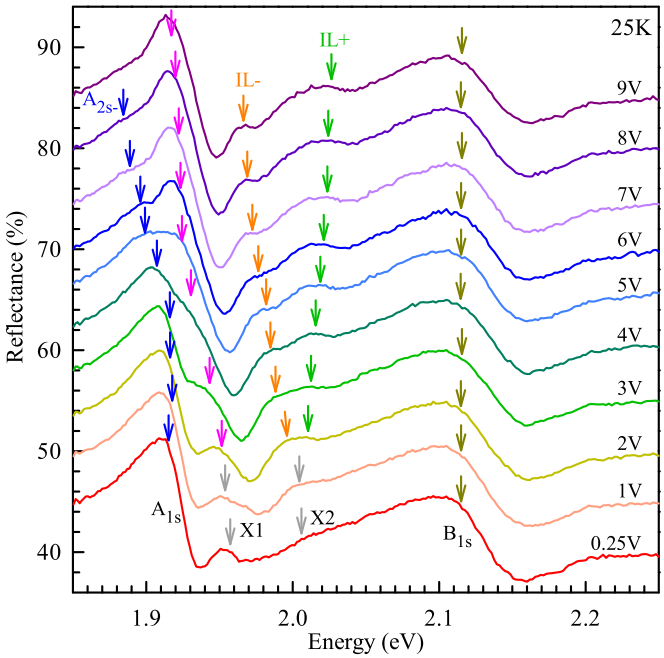

FIG. 2. Reflectance spectrum of $2H$-MoS_2 as a function of applied voltage, which results in a field $F_z \parallel \mathbf{c}$ axis. The plots are progressively shifted up by 5% for clarity.

Using the Schottky barrier formula [19] an effective electric field at the Al-MoS_2 interface can be obtained for an applied voltage. Figure 3 shows the variation of the transition energies of the different features as a function of the electric-field F_z. The continuous lines are either linear fits or, for the case marked A_{1s} and A_{2s-}, the fit is to an interacting two-level model, which reproduces the anticrossing behavior. The slope of a linear variation of the transition energy with a field reveals the dipole moment p. For features labeled IL_+ and IL_-, linear fits at high fields yield $p_{IL+} = 0.36 \pm 0.02$ enm and $p_{IL-} = -0.66 \pm 0.02$ enm. These values are similar to dipole moments measured for the interlayer exciton in bilayer $2H$-MoS_2 [11,12]. For B_{1s}, the dipole moment $p_{B_{1s}}$ is vanishingly small. For A_{2s-} and A_{1s}, using the interacting two-level model

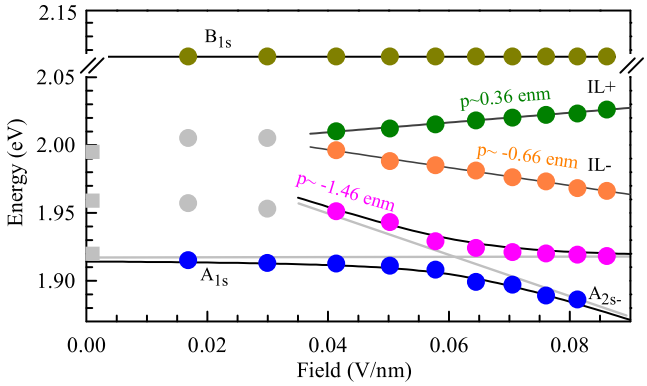

FIG. 3. Dependence of exciton transition energies on electric-field $F_z \parallel \mathbf{c}$ axis. Their identification at high fields is based on comparison with theory results. The black lines are fits, and the gray lines are a guide to the eye. The squares are data from Ref. [16].

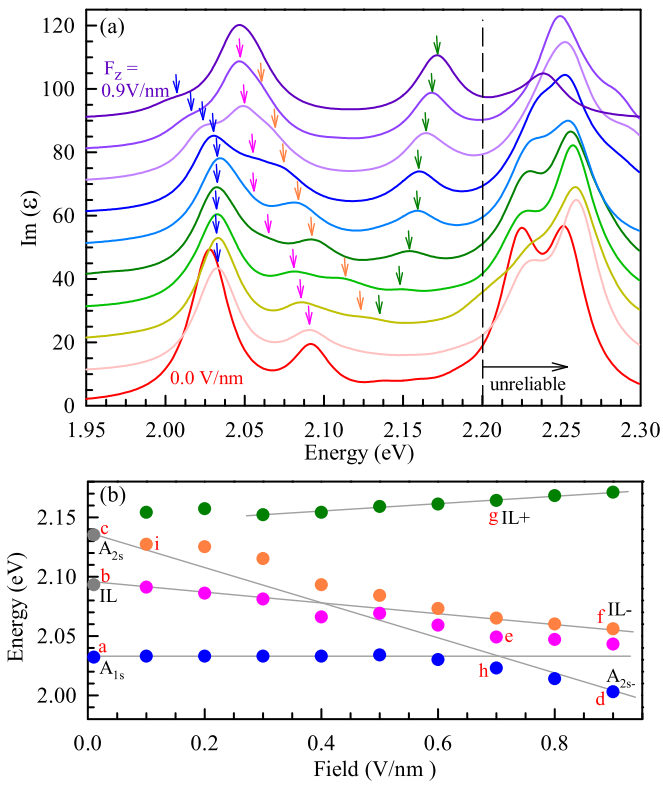

FIG. 4. Calculated (a) imaginary part of the dielectric function and (b) exciton transition energies in $2H$-MoS_2 under electric-field $F_z \parallel \mathbf{c}$ axis using GW-BSE. The lines in (b) are a guide to the eye. The points marked "a" to "i" in (b) represent exciton states for which $\overline{\chi}_s^2(z_h, z_e)$ calculated from the exciton wave function are plotted in Fig. 5.

fitting [19] with $p_{A_{1s}} = 0$ for A_{1s}, yielded $p_{A_{2s-}} = -1.46 \pm 0.03$ enm for A_{2s-}. This value of $p_{A_{2s-}}$ is more than twice as large as the interlayer exciton dipole moment reported in few-layer $2H$-MoS_2 [11–13]. A very recent study reported dipole moment of 0.73 ± 0.01 enm for interlayer excitons in bilayer and trilayer $2H$-$MoSe_2$ [20].

To understand these observations, we have performed density functional theory (DFT) based electronic band structure calculations, including the effect of the electric-field F_z. The electron-hole Coulomb interaction was included through solving the BSE [21]. Details of the calculations are given in Ref. [19]. In Fig. 4(a), we plot the theoretically calculated imaginary part of the dielectric function, which is proportional to the absorption spectrum as a function of energy for different F_z's. The peaked features represent resonant exciton absorption. With increasing F_z, they split and shift in a manner very similar to the experimental data in Fig. 2. Although the relative energies for the low-energy excitons (below 2.2 eV) are converged to about 10 meV, the absolute energies are shifted with respect to experiment as discussed in literature [28]. Also the absolute value of the fields cannot be directly compared with measurements due to the different environment of the calculation [13]. For $F_z = 0$, we find that the ground-state A-exciton A_{1s}, a new state seen in such TMD semiconductors called the interlayer exciton IL and the first excited state of A-exciton A_{2s} [8,16]. Evolution of these calculated exciton transition energies with F_z is shown in Fig. 4(b). Their trend is in good agreement with the data in Fig. 3. For finite F_z, the states IL and A_{2s} split into IL/IL_+ and A_{2s-}/A_{2s+}, respectively, and intermix as will be shown next. Note that our calculations are performed for pure $2H$-MoS_2 bulk, whereas in experiment the asymmetric dielectric environment at the metal-semiconductor interface can affect the transition energies of a split exciton pair differently. This can partially explain the observed differences with experiment.

To verify the nature of these split exciton states, we calculated the exciton wave function $\chi_S(\mathbf{r}_h, \mathbf{r}_e) = \sum_v^{\text{occ}} \sum_c^{\text{emp}} A_{vc}^S \psi_v^*(\mathbf{r}_h)\psi_c(\mathbf{r}_e)$ where the occupied (empty) band indices v (c) includes the spin and the $\mathbf{k}$ points. $\psi_{v,c}$'s are single-particle wave functions and $\mathbf{r}_h$, $\mathbf{r}_e$ are the positions of the hole and the electron. As the wave function is a complicated six-dimensional object, we focus on the z_e-z_h spatial correlation defined as $\overline{\chi}_S^2(z_h, z_e) = \int |\chi_S(\mathbf{r}_h, \mathbf{r}_e)|^2 dx_h dy_h dx_e dy_e$ in which the in-plane coordinates of the hole and electron are integrated. $\overline{\chi}_S^2(z_h, z_e)$ represents the probability of finding the hole (electron) along the z direction at z_h (z_e).

Figures 5(a)–5(i) show $\overline{\chi}_S^2(z_h, z_e)$ plotted as a function of z_e and z_h for exciton states with a specific transition energy at certain values of F_z, which were previously marked as a to i in Fig. 4(b). In the case of the ground-state exciton A_{1s} with $F_z = 0$, the electron is predominantly [8,16] in the same layer as the hole, consequently $\overline{\chi}_S^2(z_h, z_e)$ is series of bright spots along the central diagonal in Fig. 5(a) representing $z_h = z_e$. Similarly, with $F_z = 0$, for IL and A_{2s} states where the electron is expected to be mostly one and two layers away from the hole, respectively, the $\overline{\chi}_S^2(z_h, z_e)$ plot should have two series of bright spots along diagonals one and two layers away from the central diagonal, respectively, as seen in Figs. 5(b) and 5(c). For fields $F_z \neq 0$, IL/IL_+ and A_{2s-}/A_{2s+} become nondegerate, only one of the two diagonal spot series have significant weight. With this understanding, we can now identify the states in Fig. 5 as (a) A_{1s}, (b) IL, (c) A_{2s}, predominantly (d) A_{2s-}, predominantly A_{1s} with a mixture of IL_- and (e) A_{2s-}, (f) predominantly IL_-, (g) predominantlyIL_+, (h) a mixture A_{1s} and A_{2s-}, and (i) a mixture of A_{2s-} and IL_+. By comparison with these results, we identified the experimentally observed split exciton features in Figs. 2 and 3.

What we find is that with increasing F_z, there is large Stark splitting of IL and A_{2s}, the latter being much larger, but no splitting of A_{1s}. Importantly, we observe intermixing of split IL, A_{2s} and A_{1s} exciton states. We do not see a clear signature of A_{2s+} in the experimental data possibly because, unlike A_{2s-}, which mixes with a sharp and strong A_{1s} and picks up oscillator strength from it, A_{2s+} can only interact with the broad B_{1s} and is, therefore, smeared out. We underline the difference compared to previous reports on few-layer $2H$-MoS_2 where a pure IL exciton state splits under F_z and it is IL_- that blue shifts towards A_{1s} [11–13]. A very recent report on bilayer $2H$-MoS_2 shows evidence of mixing and anticrossing of IL_- with A_{1s} [22], but no mixing of A_{1s} and A_{2s-}. However, in case of bilayer $2H$-$MoSe_2$, mixing and anticrossing of A_{1s} and A_{2s} states has been reported recently [20].

In early literature, the feature $X1$ had been wrongly identified as a pure A_{2s} state [23], then as a transition at the H point

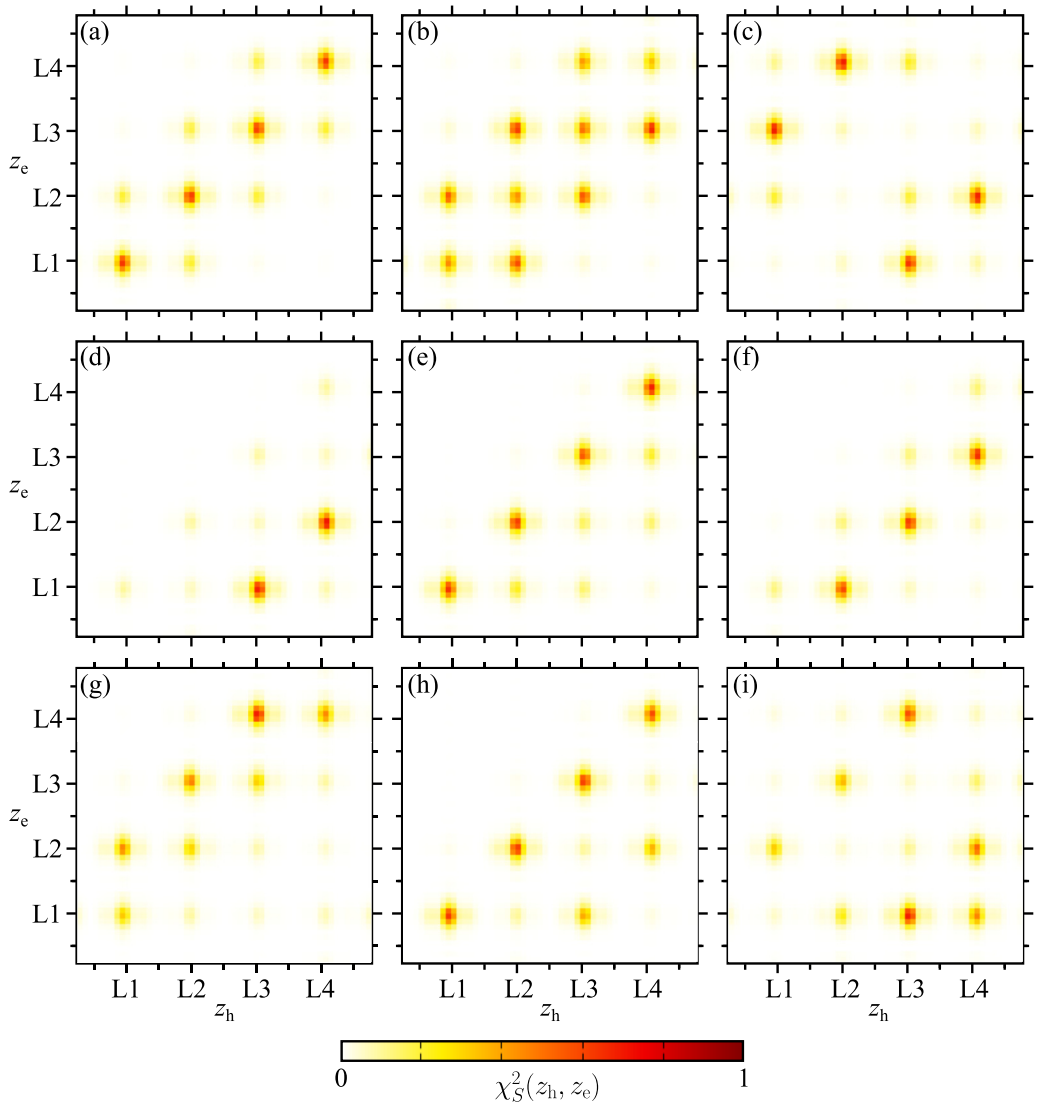

FIG. 5. (a)–(i) $\overline{\chi}_S^2(z_h, z_e)$ as a function of z_e and z_h calculated from the wave function of certain exciton states as they evolve under F_z. These states were marked in Fig. 4(b). z_e and z_h are in units of L ~0.61 nm, the distance between adjacent S-Mo-S layers in $2H$-MoS_2 along the **c** axis. For a detailed discussion of the Stark shift of pure A_{1s}, A_{2s}, IL excitons, and their mixtures, see the main text.

of the Brillouin zone [24,25] until, finally, it was understood to be a manifestation in bulk [16] of the IL exciton seen in few-layer $2H$-MoS_2 [8,10]. Now, if we trace back the energies of the exciton features identified at high F_z in Fig. 3 to low F_z, we come to the following interesting conclusion: In bulk $2H$-MoS_2, even under very weak F_z, the feature $X1$, which was most recently identified as an IL exciton, has contributions from A_{2s}, which gain strength with increasing fields, and similarly the $X2$ feature, which was thought to be a pure A_{2s}, also gains contribution from IL.

With the above identification, we can explain the measured dipole moment values. In a hydrogen atom, the $n = 1$ ground state does not possess a permanent dipole moment in first-order perturbation theory and is, therefore, not affected by an applied electric field [26]. This illustrates the insensitivity of the A_{1s} and B_{1s} ground-state excitons to F_z. However, the first excited $n = 2$ state of the hydrogen atom does possess a permanent dipole moment with magnitude $p = 3ea_0$, where e is the electronic charge and $3a_0$ is half the average distance of the electron from the origin in the $2s$ state. In contrast to highly symmetric crystals, such as Cu_2O [27] no unique a_0 can be defined in $2H$-MoS_2, which is highly anisotropic comparing in- and out-of-plane directions[8,16]. For estimating the dipole moments of IL and A_{2s}, we employ the average distance of the electron from the hole (mostly localized in the center of each layer) along the **c** axis. The highest probability of finding the electron is in the adjacent layer (at a distance of ~0.61 nm from the hole) in case of the IL state (66%), and in the next layer at ~1.22 nm in the A_{2s} state (62%) [8,16]. Accounting for these probabilities [19], we estimated the dipole moment for IL and A_{2s} to be $\sim 0.52 \pm 0.10$ and $\sim 1.3 \pm 0.2$ enm, respectively. These numbers are in fair agreement with our measured average dipole moments for the IL and A_{2s} excitons and also explain why A_{2s} with its larger electron spread along the **c** axis, has the highest dipole moment.

The A_{1s} exciton has the largest oscillator strength and shows up most prominently in reflectance. Its control with an electric field in bulk $2H$-MoS_2 would be useful for device

applications, such as tunable mirrors [7]. Normally, it is insensitive to electric-fields F_z as explained earlier. However, for the anticrossing of A_{1s} and A_{2s-}, we find the maximum sensitivity of the A_{1s} feature to F_z. This provides an indirect way of controlling the A_{1s} exciton in thicker $2H$-MoS_2 films using an electric field.

Conclusion. In conclusion, we showed that several low-energy exciton features in bulk $2H$-MoS_2 undergo very large Stark splitting in electric-fields F_z applied $\parallel$ **c** axis. We identified the different split exciton states at high fields by comparison with DFT-BSE-based calculations. We found that the A_{2s} exciton state has a dipole moment more than twice as large as the highest previously reported for an exciton species in TMDs. The results suggest that even for weak F_z, the A_{2s} and IL states are mixed in bulk $2H$-MoS_2. This adds a new perspective to the debate on the identification of the feature adjacent to A_{1s} in the absorption/reflectance spectrum of bulk $2H$-MoS_2, which had previously been attributed to a pure A_{2s} or IL transition. Although the A_{1s} exciton with the largest oscillator strength has insignificant dipole moment, its anticrossing with the Stark split A_{2s-} state leads to a change in both its oscillator strength and energy position. This can be useful for electrical control of A exciton for device applications. Furthermore, we note that Stark shifts can be expected for several excitons in other layered materials as well. Thus, electric fields are a powerful tool to disentangle their nature.

Acknowledgments. We thank V. Sugunakar and B. Chalke for technical assistance. S.G. acknowledges support of the Government of India through DAE Project No. RTI 4003. T.D. acknowledges financial support from Deutsche Forschungsgemeinschaft (DFG) through Project No. 426726249 (DE 2749/2-1 and DE 2749/2-2) and the Gauss Centre for Supercomputing e.V. for providing computing time through the John von Neumann Institute for Computing on the GCS Supercomputer JUWELS [29].

[1] K. F. Mak, K. He, J. Shan, and T. F. Heinz, Nat. Nanotechnol. **7**, 494 (2012).
[2] A. M. Jones, H. Yu, J. S. Ross, P. Klement, N. J. Ghimire, J. Yan, D. G. Mandrus, W. Yao, and X. Xu, Nat. Phys. **10**, 130 (2014).
[3] G. Wang, C. Robert, M. M. Glazov, F. Cadiz, E. Courtade, T. Amand, D. Lagarde, T. Taniguchi, K. Watanabe, and B. Urbaszek, and X. Marie, Phys. Rev. Lett. **119**, 047401 (2017).
[4] G. Wang, A. Chernikov, M. M. Glazov, T. F. Heinz, X. Marie, T. Amand, and B. Urbaszek, Rev. Mod. Phys. **90**, 021001 (2018).
[5] T. Mueller and E. Malic, 2D Mater. Appl. **2**, 29 (2018).
[6] A. Chernikov, A. M. van der Zande, H. M. Hill, A. F. Rigosi, A. Velauthapillai, J. Hone, and T. F. Heinz, Phys. Rev. Lett. **115**, 126802 (2015).
[7] P. Back, S. Zeytinoglu, A. Ijaz, M. Kroner, and A. Imamoğlu, Phys. Rev. Lett. **120**, 037401 (2018).
[8] A. Arora, M. Drüppel, R. Schmidt, T. Deilmann, R. Schneider, M. R. Molas, P. Marauhn, S. M. de Vasconcellos, M. Potemski, M. Rohlfing, and R. Bratschitsch, Nat. Commun. **8**, 639 (2017).
[9] T. Deilmann and K. S. Thygesen, Nano Lett. **18**, 2984 (2018).
[10] I. C. Gerber, E. Courtade, S. Shree, C. Robert, T. Taniguchi, K. Watanabe, A. Balocchi, P. Renucci, D. Lagarde, X. Marie, and B. Urbaszek, Phys. Rev. B **99**, 035443 (2019).
[11] E. Lorchat, M. Selig, F. Katsch, K. Yumigeta, S. Tongay, A. Knorr, C. Schneider, and S. Höfling, Phys. Rev. Lett. **126**, 037401 (2021).
[12] N. Leisgang, S. Shree, I. Paradisanos, L. Sponfeldner, C. Robert, D. Lagarde, A. Balocchi, K. Watanabe, T. Taniguchi, X. Marie, R. J. Warburton, I. C. Gerber, and B. Urbaszek, Nat. Nanotechnol. **15**, 901 (2020).
[13] N. Peimyoo, T. Deilmann, F. Withers, J. Escolar, D. Nutting, T. Taniguchi, K. Watanabe, A. Taghizadeh, M. F. Craciun, K. S. Thygesen, and S. Russo, Nat. Nanotechnol. **16**, 888 (2021).
[14] Y. Zhao, L. Du, S. Yang, J. Tian, X. Li, C. Shen, J. Tang, Y. Chu, K. Watanabe, T. Taniguchi, R. Yang, D. Shi, Z. Sun, Y. Ye, W. Yang, and G. Zhang, Phys. Rev. B **105**, L041411 (2022).
[15] N. Abraham, K. Watanabe, T. Taniguchi, and K. Majumdar, Phys. Rev. B **103**, 075430 (2021).
[16] V. Jindal, D. Jana, T. Deilmann, and S. Ghosh, Phys. Rev. B **102**, 235204 (2020).
[17] V. Jindal, V. Sugunakar, and S. Ghosh, Rev. Sci. Instrum. **93**, 023901 (2022).
[18] Y. Shimazu, T. Iwabuchi, K. Arai, and I. Shioya, Phys. Lett. A **384**, 126073 (2020).
[19] See Supplemental Material at http://link.aps.org/supplemental/10.1103/PhysRevB.107.L241201 for information on graded thickness electrode deposition, electric-field estimation, reflectance line-shape analysis, energy-level anticrossing fitting, details of *ab initio* calculations and electron probability distribution in A_{1s}, IL, and A_{2s} exciton states.
[20] S. Feng, A. Campbell, M. Brotons-Gisbert, D. Andres-Penares, H. Baek, T. Taniguchi, K. Watanabe, B. Urbaszek, I. C. Gerber, and B. D. Gerardot, arXiv:2212.14338.
[21] M. Drüppel, T. Deilmann, J. Noky, P. Marauhn, P. Krüger, and M. Rohlfing, Phys. Rev. B **98**, 155433 (2018).
[22] L. Sponfeldner, N. Leisgang, S. Shree, I. Paradisanos, K. Watanabe, T. Taniguchi, C. Robert, D. Lagarde, A. Balocchi, X. Marie, I. C. Gerber, B. Urbaszek, and R. J. Warburton, Phys. Rev. Lett. **129**, 107401 (2022).
[23] E. Fortin and F. Raga, Phys. Rev. B **11**, 905 (1975).
[24] N. Saigal, V. Sugunakar, and S. Ghosh, Appl. Phys. Lett. **108**, 132105 (2016).
[25] J. Kopaczek, M. P. Polak, P. Scharoch, K. Wu, B. Chen, S. Tongay, and R. Kudrawiec, J. Appl. Phys. **119**, 235705 (2016).
[26] D. J. Griffiths, *Introduction to Quantum Mechanics*, 2nd ed. (Pearson Prentice Hall, Upper Saddle River, NJ, 2005).
[27] T. Kazimierczuk, D. Fröhlich, S. Scheel, H. Stolz, and M. Bayer, Nature (London) **514**, 343 (2014).
[28] D. Y. Qiu, F.H. da Jornada, and S. G. Louie, Phys. Rev. Lett. **111**, 216805 (2013).
[29] D. Alvarez, Journal of large-scale research facilities **7**, A183 (2021).